INSTITUTE OF PHYSICS PUBLISHING PLASMA PHYSICS AND CONTROLLED FUSION

Plasma Phys. Control. Fusion **47** (2005) 615–634 doi:10.1088/0741-3335/47/4/003

Characterization of the deuterium recycling flux in front of a graphite surface in the TEXTOR tokamak

S Brezinsek[1], **G Sergienko**[1], **A Pospieszczyk**[1], **Ph Mertens**[1], **U Samm**[1] **and P T Greenland**[2]

[1] Institut für Plasmaphysik, Forschungszentrum Jülich GmbH, EURATOM-Association, Trilateral Euregio Cluster, D-52425 Jülich, Germany
[2] Department of Physics and Astronomy, University College, London, UK

E-mail: S.Brezinsek@fz-juelich.de

Received 24 August 2004, in final form 3 December 2004
Published 4 March 2005
Online at stacks.iop.org/PPCF/47/615

Abstract

In the TEXTOR tokamak, experiments were performed to simultaneously determine the molecular, atomic and total particle flux of deuterium in front of a graphite limiter, the temperature of which can be controlled independently of the plasma conditions. With rising limiter temperatures, T_{TL}, but constant plasma conditions an increase in Balmer emission and a decrease in Fulcher-band emission were observed. This variation is associated with a change in the type of released species: molecules dominate at low temperatures ($550\,K < T_{TL} < 1100\,K$), whereas at temperatures $T_{TL} \geqslant 1100\,K$ the direct atomic release starts to become important. The total number of deuterons remains constant for all temperatures. Since not all molecules dissociate into two potentially radiating atoms, it is necessary to take into account the ratio of atoms to molecules when deducing the total particle flux from the Balmer emission. We present a spectroscopic method which allows the determination of the atomic, molecular and total deuterium particle flux and which also gives effective conversion factors, $(S/XB)_{eff}$, to deduce the total deuterium flux from Balmer-α emission alone.

Analysis of the spectroscopic data of both species can be performed to determine the rotational and vibrational populations for the molecules by means of Fulcher-α spectroscopy, and the penetration depth and energy for the atoms using Balmer spectroscopy. This further analysis gives additional information about the release mechanism, showing that both species, atoms and molecules, are released predominantly as thermalized particles.

(Some figures in this article are in colour only in the electronic version)

1. Introduction

Hydrogen isotopes are the fuelling gases in fusion devices. Their behaviour in front of plasma-facing components (PFCs), such as walls, limiters and divertors, is of major interest [1, 2]. Apart from the atomic species, molecular species are also present in the plasma edge region in front of PFCs [3, 4]. The fluxes of these species released from PFCs, as well as their velocity distributions, relative concentrations and lifetimes, are the important quantities. All these quantities are covered by the generic term 'hydrogen recycling' [5–8] and are of special interest for particle control in fusion devices. For molecules, the magnitude of the vibrational ground state population is of importance since it can vitally influence the recycling process [9].

Passive spectroscopy of atomic lines is a standard method for determination of atomic particle fluxes, Γ_A. The conversion of photon fluxes, ϕ_A, takes place by means of inverse photon-efficiencies or S/XB values for the observed electronic transition of the atom: $\Gamma_A = S/XB \cdot \phi_A$. In the same manner, the determination of the molecular flux, Γ_M, can also be accomplished with the help of so-called D/XB values and the photon fluxes, ϕ_M, deduced from all rovibrational lines of the observed electronic transition: $\Gamma_M = D/XB \cdot \phi_M$. In the case of hydrogen, the lines of the Balmer series (α, β, γ, ...) are usually observed to determine the atomic hydrogen particle flux [10] and the Fulcher-α band is used to determine the molecular flux [11, 12].

Fulcher-α spectroscopy also provides information about the rotational and the vibrational populations of molecules in the excited electronic state $3p\,^3\Pi_u$. The mapping from this electronically excited state into the electronic ground state requires collisional–radiative models [13, 14]. These collisional–radiative models for hydrogen provide modified D/XB values for one electronic transition and include level mixing and cascading processes.

We present measurements in deuterium discharges performed in front of a pre-heated graphite test limiter positioned in TEXTOR. Depending on the surface temperature, a change in the ratio of molecular to atomic deuterium flux has been observed using passive spectroscopy. These measurements have been made mainly on the Fulcher-α band and the Balmer-α and -γ transition of deuterium.

Atoms and molecules contribute to the total number of deuterons, and therefore both species have, in principle, to be measured simultaneously to determine the total released deuterium particle flux, Γ^{tot}, given by $\Gamma^{tot} = \Gamma_D + 2\Gamma_{D_2}$. Since the atoms arise partially from the dissociation of molecules, an exact determination of the molecular and the atomic contributions to the deuterium recycling flux is mandatory to avoid any double counting of the resulting deuteron flux. Additionally, for a better understanding and for comparison with the model, information about the energy distribution of the break-up products as well as about the penetration depth of the atomic and molecular species and about their variation with the surface temperature is necessary.

The experimental setup is described in section 2, and the experimental results are presented in section 3. A detailed analysis of the results is given in section 4, and a simple model for the release mechanism in dependence on the surface temperature will be discussed. Finally, effective inverse photon efficiencies are presented, which allow determination of the total deuterium particle flux from the line emission of Balmer-α.

2. Experimental setup

The medium-sized tokamak TEXTOR ($R = 1.75\,m$, $a = 0.46\,m$) is described in detail elsewhere [15]. TEXTOR was operated under the following conditions: $I_p = 350\,kA$, $B_t = 2.25\,T$. The working gas was deuterium. Hydrogen neutral beam heating was only

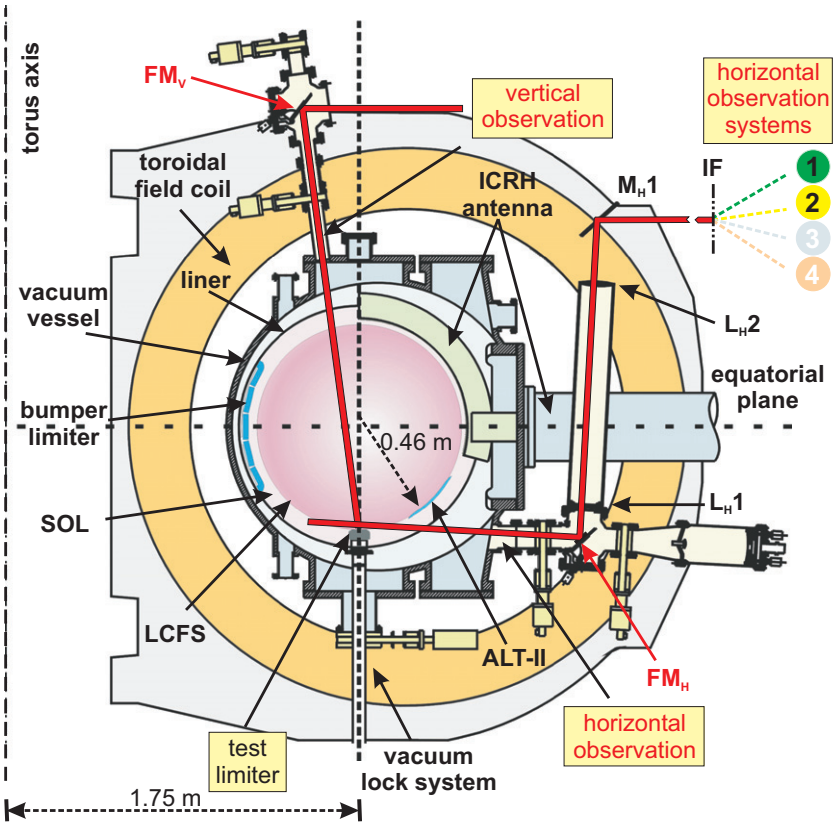

Figure 1. Poloidal cross section of TEXTOR. The vacuum lock system, housing the test limiter, the vertical observation port and the horizontal observation port are located at the same toroidal position. The optical paths for both observation systems are indicated. L_H1, the first lens of the horizontal observation path, is also used as a window to the vacuum vessel.

used in the start-up phase of the discharge and provided an additional power of 1.3 MW to the plasma during this time. However, the measurements were made in the ohmic phase of the discharge. The boronized first wall (liner) was actively pre-heated to a temperature of 620 K which allows a better control of the global plasma parameters and of the hydrogen exhaust.

The experiments were performed in front of a graphite test limiter (TL). The TL is part of a spherical sector made of graphite (EK98) with a curvature of 0.07 m and a base of 0.12 m $\times$ 0.08 m. This limiter was located in a vacuum lock system at the bottom of the torus (figure 1) and positioned at the last closed flux surface (LCFS).

The LCFS itself was determined by the main toroidal belt limiter, ALT-II, at $r = 0.46$ m, which is also made of graphite. The geometry of the TL and the area ratio between the TL and ALT-II limiter led to a heat flux towards the TL of 3–8% of the total heat flux flowing into the scrape-off layer (SOL). One part of the poloidal limiter ($r = 0.47$ m)—located at the bottom of the torus in the adjacent toroidal section—shadows the TL slightly, whereas the influence of the bumper limiter—located on the high-field side at $r = 0.51$ m and toroidally circumferential—is negligible. This shadowing leads to a minor reduction of the total influx on the TL.

The graphite limiter bulk was actively pre-heated by an electric heating plate system (figure 2(a)), which provided a homogeneous temperature distribution in the bulk and on the surface independently of an inhomogeneous heating by the plasma. The heating plate consists

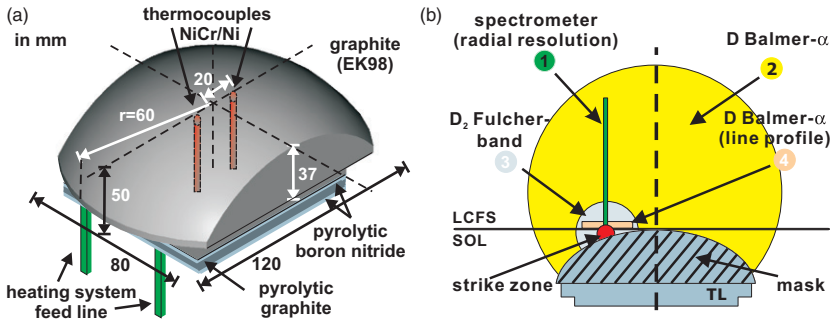

Figure 2. (*a*) The electrically pre-heatable limiter TL. (*b*) Side view of the TL. The observation areas are indicated.

of a combination of pyrolytic boron nitride and pyrolytic graphite layers. A homogeneous surface and bulk temperature with a maximum value of 1500 K can be achieved ($P_{\mathrm{H}} \geqslant 3.5$ kW). Two Ni/CrNi thermocouples, 15 mm away from the tip of the limiter on both sides in the toroidal direction and located 2 mm below the surface, were used for an *in situ* temperature measurement. Two observation ports were employed for the experiment: a vertical port and a horizontal port, both depicted in figure 1.

Horizontal view. Multiple spectroscopic measurements were performed by means of the horizontal observation port. The line of sight is directed tangentially on the limiter, and four spectroscopic systems were utilized for simultaneous observation. The optical paths, shown in figures 1 and 3, are nearly identical for all systems and include two plane folding mirrors: FM_{H} and $M_{\mathrm{H}}1$.

The TL is imaged by the lens $L_{\mathrm{H}}1$ on an intermediate image plane where $L_{\mathrm{H}}2$ is positioned. $L_{\mathrm{H}}2$ works as a field lens for an optimized light exploitation and images $L_{\mathrm{H}}1$ on an intermediate image field (IF). At the IF a splitting of the optical path for an adaptation to each individual detection system is performed. Thereby systems 1 and 2 produce a direct image of the TL on the detection system, whereas an indirect image is made by use of a light guide system on 3 and 4.

- System 1: The lens $L_{\mathrm{H}}3$ is used for a further image of the TL on the 50 μm entrance slit of a 0.5 m imaging spectrometer (Acton Research Corporation, model SpectraPro 500) with a holographic grating (68 mm × 84 mm, 2400 lines per millimetre) in Czerny-Turner arrangement. The time resolution of the system is determined by a two-dimensional camera (Proxitronic, model RL4) to 40 ms. The size of the CCD array is 756 × 581 pixel with an individual pixel size of 11 μm × 11 μm. The camera is equipped with an image intensifier of MCP type (Proxifier with S20 cathode), which is coupled to the CCD by means of a 25 : 11 optical UV fibre taper. The system routinely covers the wavelength range between 425 and 435 nm in the first order, including the strongest band of *CD* ($A\,^2\Delta \rightarrow X\,^2\Pi$) and Balmer-$\gamma$, and provides a spectral resolving power, $\lambda/\Delta\lambda$, of about 7000 at 430 nm. The system has a radial resolution of about $\Delta r = 0.2$ mm.
- System 2: Part of the light from the main optical path is deflected by mirror $M_{\mathrm{H}}2$ and directed onto a two-dimensional CCD camera (Proxitronic, model RL4) with an image intensifier of MCP type (Proxifier with S20 cathode). The image intensifier and CCD are coupled via an 18 : 11 optical UV fibre taper. The camera was equipped with an interference filter for the Balmer-α line (656.3 nm, FWHM = 3.0 nm). System 2 was utilized for the measurement of the radial and toroidal distribution of the light emission

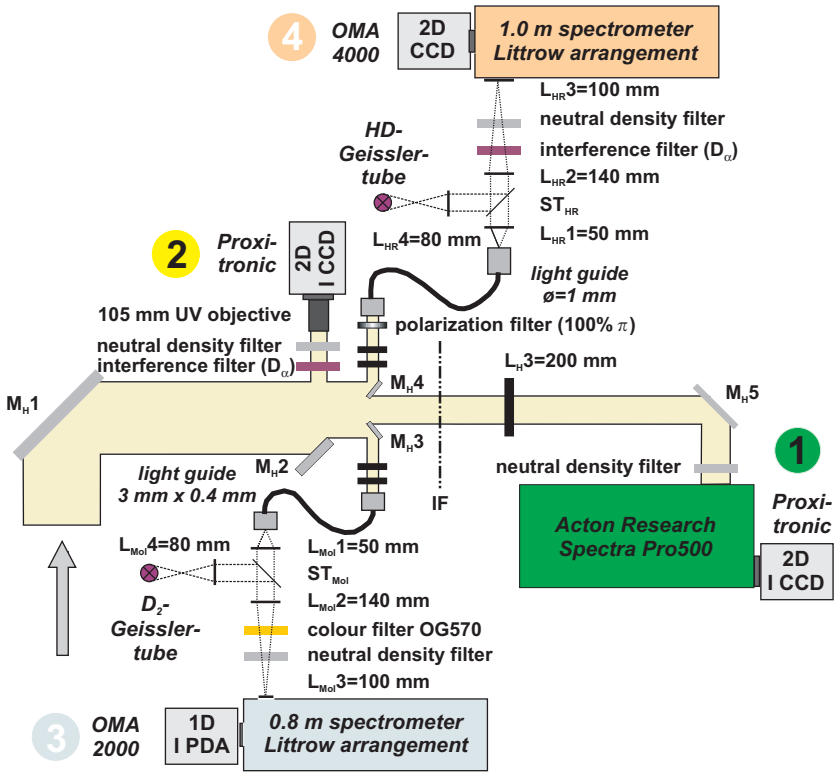

Figure 3. Schematic view of the optical paths for the four observation systems located at the horizontal diagnostic port.

of deuterium atoms in front of the TL. The spatial resolution of the camera system was determined to 0.5 mm with the objective used (Nikon, model UV-Nikkor 105 mm).

- System 3: Part of the light of the main optical path is deflected by mirror $M_{\mathrm{H}}3$, coupled into a quartz optical fibre, and finally, by means of a lens system, imaged onto the entrance slit (50 μm) of a 0.8 m spectrometer in Littrow arrangement. The spectrometer, which functions on the principle of auto-collimation, is equipped with a single apochromatic lens (150 mm diameter) in front of the Echelle grating. The Al-coated grating (165 mm $\times$ 150 mm), with a blaze angle of 46°, was ruled with 1200 grooves per millimetre. An optical multichannel analyser system (EG&G Princeton Applied Research, model OMA 2000), which consists of an intensified linear diode array (model 1421) with 1024 pixels and a detector controller (model 1461), was used for detection. Each pixel of the array is 25 μm wide and 2.5 mm high. The detector was cooled to -10°C, and the exposure time was set to 200 ms.

  The spectrometer was operated in second order. The resolving power, $\lambda/\Delta\lambda$, of the system, which was experimentally determined by the measurement of an effective Gaussian instrumental line profile with the aid of a Geissler discharge tube, is approximately 13 000 at 600 nm. The wavelength range covered amounts to 8 nm in one recording. System 3 observed the strongest band emission of molecular deuterium (Fulcher-band).
- System 4 is similar to system 3. The shape of the Balmer-α line was measured with the aid of a 1 m spectrometer in Littrow arrangement. An optical fibre bundle was used

to transmit that part of the light to the entrance slit of the spectrometer with an Echelle grating which was deflected from the main optical path by M_H4. The spectrometer was equipped with a single apochromatic lens with a diameter of 130.0 mm. The Echelle grating (220 mm × 110 mm), with a blaze angle of 76°, had 79 lines per millimetre.

The spectrometer system was operated in the 37th order and provided a high resolving power of about $\lambda/\Delta\lambda = 90\,000$ at 656.3 nm. To avoid order mixing, a narrowband interference filter (656.3 nm, FWHM = 3.0 nm) was used as a pre-dispersive element in front of the 50 μm entrance slit. In addition, a polarization filter ensured that only the π-components of the Zeeman-split line were observed.

A two-dimensional OMA system (EG&G Princeton Applied Research, model OMA 4000), which consists of a Peltier-cooled (−60°C) CCD camera (model 1530) and a controller unit (model 1533), was deployed for detection. The non-intensified camera had a CCD array with 512 × 512 pixels and each pixel had an area of 19 μm × 19 μm. Owing to the low photon efficiency of the system, the integration time was fixed to 1 s during the experiment.

The depth of focus of the main optical image is large enough to ensure that a sharp image is obtained over the whole width of the TL. The observation areas of the four systems are the projection of this sharply focused region onto the plane shown in figure 2(*b*). The observation areas of systems 1, 3 and 4 are directly located at the strike zone of the limiter. As previous investigations—performed with system 2 and an interference filter for the first diagonal transition of the Fulcher-band ($\lambda = 601.5$ nm, FWHM = 3.0 nm)—have shown, the observation area of system 3 is large enough to ensure that all photons emitted from the D_2 molecules are detected [16]. Owing to the large penetration depth of the atoms into the TEXTOR plasma (see [17] and section 3.3), we have used a larger observation area (system 2) to observe the total Balmer-α emission than we use to observe the molecular light emission. For the absolute comparison of released particle fluxes, only the ion drift side, as indicated in figure 2(*b*), was employed.

In contrast to previous experiments [18], a mask was positioned in front of the field lens L_H2 to prevent detection of the thermal background during the strong external heating phase of the TL. The mask was optimized for the size of the side view projection of the TL and fixed at the same place for the whole experiment. In figure 2(*b*), the area covered by the mask is indicated by the diagonally hatched area.

Vertical view. The observation of the limiter surface and an additional measurement of the TL surface temperature were performed by means of the vertical observation system. Therefore, an IR-sensitive CCD camera (Hitachi, model KP-M1, 756 × 581 pixels) equipped with a high-pass optical filter with a transmission above 0.85 μm was used. We also determined the surface temperature using Planck's law from these measurements and compared the values with the results from the thermocouples which were used as the reference values for the TL temperature. The temperatures from the grey-body calculations are only available above 850 K and they are about 30–50 K higher than the values deduced from the thermocouples.

3. Experimental results

The main aim of these experiments was to determine the total deuterium particle flux released from graphite for a specific set of plasma parameters. A variation of the limiter temperature, T_{TL}, generated by external electrical heating, was performed in two series of both 17 and 16

Table 1. Local plasma parameters at the LCFS and the range of achieved limiter temperatures for the two types of discharge series.

Series	Discharge	n_e [10^{18} m^{-3}]	T_e [eV]	T_i [eV]	T_{TL} [K]
1	89133–50	2.8	77	120	620–1380
2	89155–70	5.2	42	150	570–1390

nearly identical plasma discharges. The plasma parameters were kept constant for a phase of at least 1 s of the discharge. In series 2, in comparison with series 1, the local edge electron density, n_e, is almost doubled and the local edge electron temperature, T_e, is nearly halved. n_e and T_e for these two types of discharges were measured using a He atomic beam diagnostic. This diagnostic is located at the midplane the low-field side of the torus and shifted 45° in toroidal direction [19], but still situated on the same flux surface as the TL. The ion temperature has been determined by means of charge-exchange spectroscopy on fully ionized carbon at the hydrogen diagnostic beam placed in the adjacent toroidal section [20] on the midplane of the high-field side. The plasma parameters at the LCFS for the two series are given in table 1.

The externally controlled temperature of the limiter was varied from discharge to discharge (table 1). T_{TL} was held constant for at least 1 min, except for 570 K, which represents a transient temperature due to the higher surrounding temperature of the liner. Only a minor increase in the homogeneously distributed temperature could be found by means of thermography in the later phase of the discharge. We assume that in the first part of the plateau phase which was used for the measurement, a negligible increase of T_{TL} occurs owing to the plasma itself.

3.1. The deuterium Balmer-α and Fulcher-band photon flux

The photon flux from atomic deuterium, ϕ_D, measured as D_α light, shows a nearly constant value up to a temperature of about 1100 K for both series. For T_{TL} higher than 1100 K, a significant increase in ϕ_D of more than 50% at the maximum measured T_{TL} is detected. Similar results were found in the observation of the D_γ intensity (section 3.3).

The photon flux from surface-released molecules, ϕ_{D_2}, was measured simultaneously via the line intensities of the Fulcher-α band ($3p\,^3\Pi_u \rightarrow 2s\,^3\Sigma_g^+$). In previous experiments [18] we used this method for determination of the molecular particle flux as a function of the local plasma parameters in front of a similar, but not actively heated, limiter ($T_{TL} = 620$ K). By means of these experiments we could deduce scaling factors $c(n_{0,0} \rightarrow n_{v,v'})$ which provide the extension of the photon flux of the first diagonal vibrational band to all diagonal bands in dependence on the local plasma parameters. Furthermore, the branching ratios for non-diagonal transitions were included and a reduction of the total number of discharges to cover the whole wavelength range of Fulcher-band emission from six to only one was achieved. This measurement as well as the full method is described in detail in [18]. In the present experiment we apply this knowledge to determine ϕ_{D_2} using the photon flux of the first diagonal transition multiplied by the scaling factors for the plasma parameters used.

As seen in figure 4, ϕ_{D_2} shows a decrease in the light emission of about 50% in the temperature range between 1100 and 1400 K, which is the behaviour opposite to that of ϕ_D. A complete disappearance of the molecular intensity for $T_{TL} > 1750$ K in the first discharge series and for $T_{TL} > 1700$ K in the second series can be expected when the curve is extrapolated to higher temperatures. For technical reasons, such a high T_{TL} could not be reached. The change in ϕ_{D_2} at about $T_{TL} = 1100$ K is thus just as sharp as for ϕ_D. Up to this value, the variation of the flux is practically negligible for both discharge conditions. The corresponding particle fluxes are determined and analysed in section 4. Similar results showing the same sharp

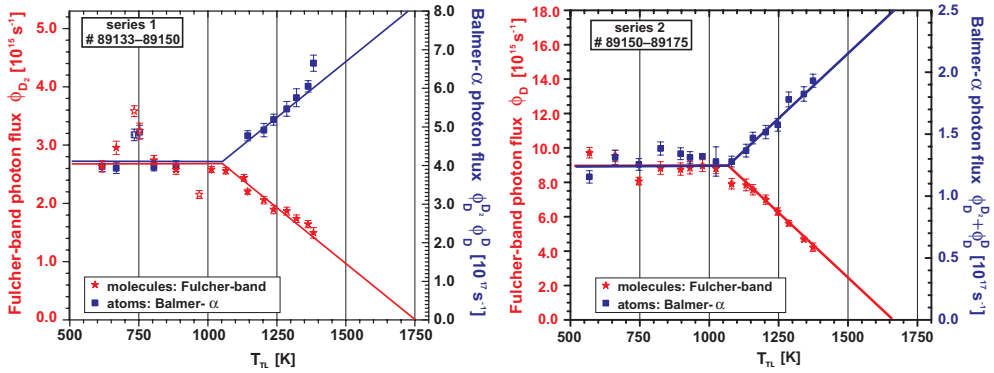

Figure 4. Variation of the Balmer-α and the Fulcher-band photon flux for the two discharge series. The behaviour is similar for both series: an almost constant phase up to $T_{TL} \approx 1100$ K, a nearly linear increase in ϕ_D and a nearly linear decrease in ϕ_{D_2} for higher temperatures. Minor discrepancies in series 1, marked by the open squares and stars, can be attributed to slight changes in the local plasma parameters.

transition for atoms and molecules were obtained earlier at similar temperatures from deuterium ion beam experiments on carbon surfaces [21].

3.2. Molecular properties

Additional information about the influence of the limiter temperature on the distribution of the released molecules can be deduced from the analysis of the rotational and vibrational populations of D_2. Thus, a possible redistribution of the initial vibrational and rotational populations within the variation of T_{TL} is taken into account. Direct information from passive spectroscopy in the visible part of the spectrum can be obtained only on the electronic excited state $3p\,^3\Pi_u$. However, a calculation of the population in the electronic ground state, $1s\,^1\Sigma_g$, from the excited electronic state is possible [22, 23].

The rotational population was determined by a Boltzmann plot of the Q lines of the first main diagonal branch. Six lines were included in the fitting procedure for the rotational temperature in the excited state, $T_{rot}^{(3p\,^3\Pi_u, v=0)}$. No deviation from a Boltzmann distribution has been observed for these lines. The dependence of $T_{rot}^{(3p\,^3\Pi_u, v=0)}$ on T_{TL} for both discharge series is depicted in figure 5. The $T_{rot}^{(3p\,^3\Pi_u, v=0)}$ values for corresponding values of T_{TL} are well-separated for both series: for the larger local electron density a slightly higher rotational temperature is obtained. This confirms previous measurements which have revealed an electron density dependence of the rotational temperature in the plasma parameter range covered in TEXTOR [24].

Figure 5(*a*) also shows a variation of $T_{rot}^{(3p\,^3\Pi_u, v=0)}$ with increasing T_{TL} without a change in the local plasma parameters. A similar linear dependence of $T_{rot}^{(3p\,^3\Pi_u, v=0)}$ has been observed in reference D_2 gas-puff experiments in TEXTOR, where the initial gas temperature, $T_{initial}$, was varied over a large temperature range [24]. To parametrize both dependences, we can use the following expression for the ground state rotational temperature: $T_{rot}^{(1s\,^1\Sigma_g, v=0)} = T_{initial} + \Delta T(n_e, T_e, \ldots)$. This equation can be transferred into the excited state by taking the ratio of the molecular constants ($B_{(3p\,^3\Pi_u, v=0)}/B_{(1s\,^1\Sigma_g, v=0)} \simeq 0.50$) into account [25]:

$$T_{rot}^{(3p\,^3\Pi_u, v=0)} = [T_{initial} + \Delta T(n_e, T_e, \ldots)] \frac{B_{(3p\,^3\Pi_u, v=0)}}{B_{(1s\,^1\Sigma_g, v=0)}}. \quad (1)$$

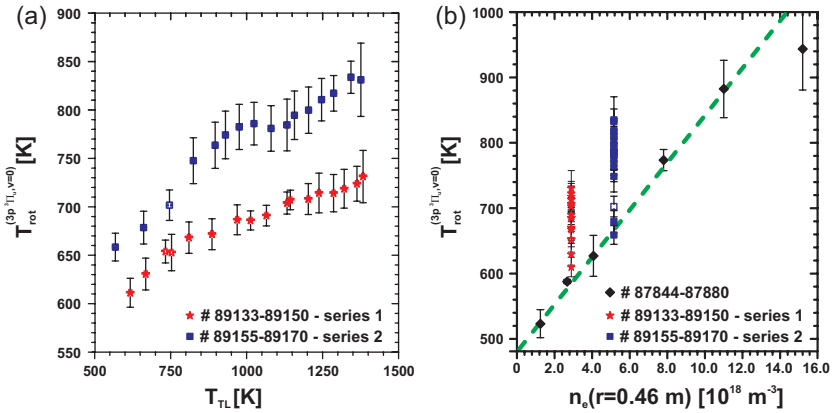

Figure 5. (*a*) The rotational population temperature, $T_{\mathrm{rot}}^{(3\mathrm{p}\,^3\Pi_\mathrm{u},v=0)}$, deduced from the Q-branch of the first diagonal vibrational transition for the two discharge series as a function of T_{TL}. (*b*) $T_{\mathrm{rot}}^{(3\mathrm{p}\,^3\Pi_\mathrm{u},v=0)}$ for both series as a function of n_e at the LCFS. The series #87844–87880 (- - - -) represent an electron density scan with almost constant T_{TL} at 620 K.

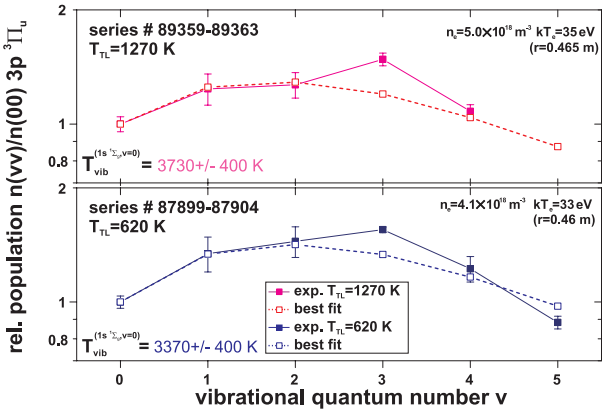

Figure 6. The relative vibrational population in the excited electronic state for two discharge series at $T_{\mathrm{TL}} = 1270\,\mathrm{K}$ (top) and $T_{\mathrm{TL}} = 620\,\mathrm{K}$ (bottom). The limiter temperature is kept constant in both cases, but all other experimental conditions for the two discharge series (top #89359–89363 and bottom #87899–87904), i.e. the plasma edge parameters, are comparable to those of discharge series 2.

In the present case only T_{initial} has been modified and $\Delta T(n_\mathrm{e}, T_\mathrm{e}, \ldots)$ remains constant within one series of discharges. The nearly linear increase in $T_{\mathrm{rot}}^{(3\mathrm{p}\,^3\Pi_\mathrm{u},v=0)}$ with T_{TL} is thus determined by the increase in T_{initial} only, which can then be identified as the gas temperature of the released molecules. However, between 950 and 1150 K a small plateau is created, whose origin is probably a local density variation and thus a small change in $\Delta T(n_\mathrm{e}, T_\mathrm{e}, \ldots)$ due to the break-up of hydrocarbons [16].

The relative vibrational population of $3\mathrm{p}\,^3\Pi_\mathrm{u}$ for two similar plasma conditions, but two different surface temperatures, is given in figure 6. In contrast to the rotational population, the vibrational population shows only a minor variation with a change of T_{TL}. The variation of the scaling factors, $c(n_{0,0} \rightarrow n_{v,v'})$, mentioned in the previous section, is almost negligible within this change of the vibrational population with T_{TL}. The best-fit equivalent ground state

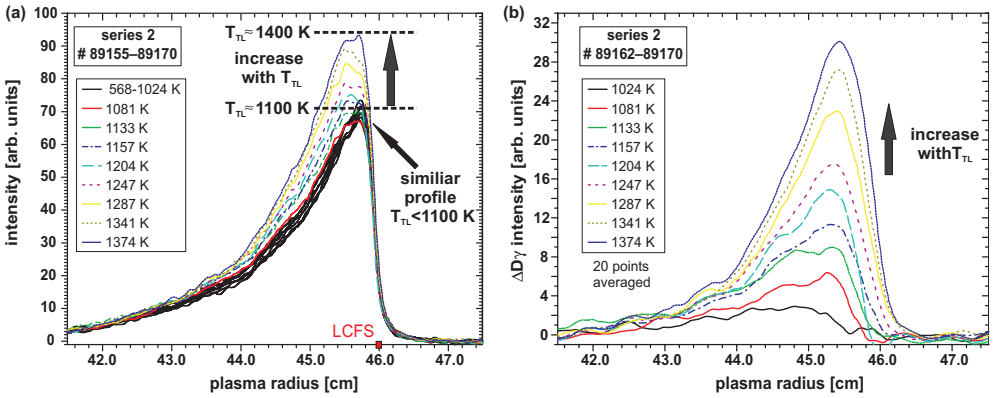

Figure 7. (*a*) Variation of the D_γ radial intensity distribution with an increase in the limiter temperature. (*b*) Relative change in the D_γ intensity for $T_{TL} > 1100$ K.

population, which was calculated from the excited state by means of effective Franck–Condon factors deduced using the CRMOL code [23], is also depicted. The reason for the deviation of the population of the upper $v = 3$ state is still under investigation.

An ansatz similar to that for $T_{rot}^{(1s\,^1\Sigma_g, v=0)}$ can be used for $T_{vib}^{(1s\,^1\Sigma_g)}$, but in the case of the vibrational population the plasma parameter term dominates strongly over the term for the initial vibrational temperature of the D_2 molecules. However, the difference between the $T_{vib}^{(1s\,^1\Sigma_g)}$ measurements is small and lies within the experimental error: thus, we neglect the variation of the ground state population during the heating.

3.3. Atomic properties

To characterize the atoms, the penetration depth and the energy distribution were measured by means of Balmer spectroscopy performed with system 1, observing D_γ, and system 4, observing D_α. These measurements clearly show a variation of these atomic properties with a change in the limiter temperature although the plasma is kept constant.

The penetration depths of atomic and molecular species have already been observed in front of limiters in TEXTOR [26–28]. For a variety of plasma parameters these measurements have shown that the penetration depth of D_2 is of the order of a few millimetres and that of D is of the order of several centimetres. The emission maximum of atoms and molecules varies in the radial direction owing to the production of atoms dissociated from molecules. However, the present experiment shows that the penetration depth of atoms, λ_D, is not determined by the plasma conditions only.

λ_D can generally be described as a function of the electron density, n_e, the rate coefficient for ionization, $\langle \sigma v_e \rangle$, and the atomic velocity, v_D. The first two quantities cover the part of λ_D which mainly depends on plasma parameters and which remains constant within different discharges of a series. v_D represents the part of λ_D which is determined by the origin of the atoms (dissociation process, thermal release . . .).

The radial distribution of D_γ is depicted in figure 7(*a*) as a function of T_{TL} for series 2. The radial D_γ emission profiles are similar up to a threshold temperature of about 1100 K and can be characterized by two e-folding lengths of about $\lambda_1 \simeq 17$ mm at the wings and $\lambda_2 \simeq 13$ mm close to the maximum. Note that the measured radial distribution represents a convolution of different radial profiles owing to the curvature of the limiter; also, high

energetic atoms are not completely covered by the observation volume of system 1 (section 2). A significant modification of the distribution takes place above the threshold and the D_γ intensity grows continuously with increasing T_{TL}.

The active heating of the limiter changes the velocity distribution of the atoms which emit Balmer radiation. To illustrate the increase in the radial distribution, we subtract the D_γ emission profile at the lowest T_{TL} from the profiles at higher temperatures (figure 7(*b*)). Clearly, a new atomic velocity class, with its radial maximum of emission next to the limiter, appeared at higher temperatures. The penetration depth, λ_2, drops to about 11 mm at about 1400 K and represents now a mixture of two 'low speed' atomic species.

An analysis of the energy components of the atomic species at one radial position is performed in the next section. As we shall see, this new velocity class can be attributed to thermalized atoms which are directly released from the surface of the pre-heated limiter. The larger penetration depth can mainly be attributed to atoms which arise from molecular dissociation and thus from a displaced volume source. Laser-induced fluorescence measurements of Lyman-α at the same type of pre-heated limiter confirmed this [27].

Integration over the radial distribution provides an intensity value proportional to the D_γ photon flux. The variation of the D_γ intensity as a function of the limiter temperature is in good agreement with the change in the D_α light. A closer look at series 2 shows the similarity: a constant value up to a threshold of 1100 K and a nearly linear increase of about 45% of the intensity between 1100 and 1400 K. This is similar to the D_α variations presented in section 3.1. A comparison of the absolute photon fluxes is not possible due to the restricted observation volume for D_γ.

The line profile analysis of D_α, recorded using system 4, also provided information about the new atomic component which appeared at a high T_{TL}. The line shape has been simulated by means of theoretical profiles, calculated on the basis of the 20 Zeeman-split π-components of D_α [29], convoluted with the apparatus function of the detection system and with Doppler-profiles which correspond to certain energies as we now describe [30, 31]. Three temperature components were identified for cold limiter conditions ($T_{TL} = 620$ K). First, a single Gaussian curve, representing a high energetic component, was fitted to the blue wing of the D_α line profile shown in figure 8. This broad component can be attributed to reflected and charge-exchange particles. The fitting of the profile at the far wing is relatively insensitive due to the low intensity, and therefore, the fitted energy ($kT_h \simeq 90$ eV) is flawed with larger uncertainties. The ion temperature at the LCFS (table 1) gives an upper limit for the energy of species of this velocity class. The energy and fraction of the broad component are only determined by the plasma edge and remain constant with increasing limiter temperature.

In a second step, the broad component was subtracted from the initial D_α line profile, and a detailed fit of the residual profile in the central region, confined by the dashed lines in figure 8, was performed. Two Gaussian curves representing a cold component ($kT_c \simeq 0.25$ eV) and a lukewarm component ($kT_l \simeq 3.4$ eV) were necessary to fit the residual profile. The energy of both narrow components and their individual fractions are determined by a least-square fit routine. These low energy components can be attributed to deuterium atoms whose origin is the molecular dissociation upon electron impact. Different dissociation processes, which will be briefly discussed below, can produce atoms with the characteristic energies of the two narrow components.

In contrast to the broad component, the fraction and the energy of the narrow components depend on the temperature of the limiter. The temperature of the cold component varies in a manner which mirrors the variation of the Fulcher-band photon flux depicted in figure 4. Up to the threshold temperature of $T_{TL} = 1100$ K, only a minor variation of the temperature

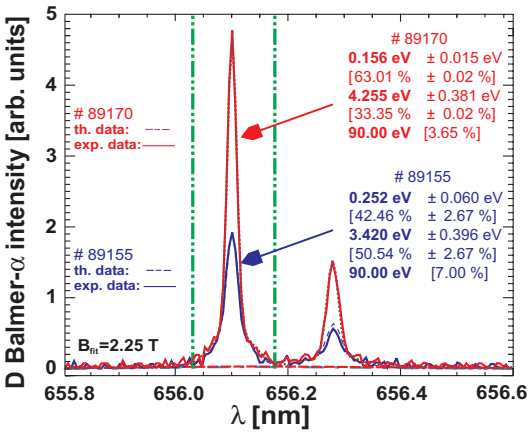

Figure 8. Analysis of the π-components of the Balmer-α line for discharges with a low (#89155) and a high (#89170) limiter temperature.

of the cold component[3] could be observed with $kT_c = 0.25$ eV rising to 0.30 eV. In the limiter temperature range below the threshold, the measurement shows almost no variation in the atomic distribution among the three components. Above the threshold, however, the distribution changes significantly. kT_c decreases continuously to 0.16 eV at $T_{TL} = 1400$ K as depicted in the second fit in figure 8, labelled as #89170. In addition, the fraction of this component increases from 43% up to nearly 63%, whereas the amount of the lukewarm component decreases from 50% to 33%. At the same time kT_l increases at high T_{TL} up to 4.3 eV.

At limiter temperatures above $T_{TL} = 1100$ K, the component kT_c can also be interpreted as a mixing of two cold components. The energy of the first cold component remains unchanged at about 0.30 eV in all discharges with limiter heating. Its fraction is nearly constant up to the threshold of $T_{TL} = 1100$ K, but decreases linearly with higher T_{TL} and probably disappears at about 1700 K, where the molecular emission (section 3.2) also vanishes. This cold component can be attributed to atoms from molecular dissociation. The second cold component represents thermal atoms which are released directly from the surface with T_{TL}. This component appears above $T_{TL} = 1100$ K and its fraction increases in opposition to the decrease of the first cold component. The reduction of the fraction of the lukewarm component at elevated limiter temperatures is in line with the reduction of the molecular source. Thus the overall increase in percentage of the mixed cold component can be attributed to an additional source of thermalized atoms.

An overview of possible molecular dissociation reactions with an analysis of the break-up products is presented in [32] for the parameter range of a high temperature plasma edge. Here, the electron impact-induced dissociation process $D_2 + e^- \rightarrow D + D + e^-$ (type (i) reaction), which has the lowest threshold energy of about 8.9 eV, can already be excluded because of the energy of the atomic fragments. Each atom should reflect the Franck–Condon energy of about 2.2 eV, but atoms with such energies were not observed in the experiment. Two types of dissociation reactions were pointed out as the most probable for explaining the experimentally observed narrow components [31]: $D_2 + e^- \rightarrow D^* + D^+ + e^- + e^-$ (type (ii)) and

[3] Similar temperatures for the cold component were found in earlier measurements [30] performed close to the wall ($T = 620$ K) on the outer midplane of TEXTOR. The observation was parallel to the magnetic field and the 34 σ-components of D_α were recorded.

$D_2 + e^- \rightarrow D + D^* + e^-$ (type (iii)) which include excitation into the electronic states $n = 2$ and $n = 3$. The local electron temperature is above the threshold energy, which is below 18.0 eV for the reactions of type (ii) and (iii).

4. Determination of the total deuterium particle flux

4.1. A scheme for interpretation of the deuterium photon fluxes

The final step towards the determination of the total released deuterium particle flux, Γ^{tot}, and its composition is the conversion of the photon fluxes presented in section 3 into particle fluxes. As atoms and molecules contribute to the total number of deuterons, we have to omit any double counting of the deuterons. Γ^{tot} can be written as

$$\Gamma^{\mathrm{tot}} = \Gamma_{\mathrm{D}} + 2 \cdot \Gamma_{\mathrm{D}_2} = \Gamma^0_{\mathrm{D}}, \tag{2}$$

where Γ^0_{D} is identical to the total flux of the resulting deuterons. The limiter is fully saturated within several milliseconds [16] and a complete recycling takes place on the surface. In this case, the number of ions set free from the surface is negligible [21] and thus the recycling coefficient for deuterium is unity. The incoming ion flux, Γ^+_{D}, is identical to the flux of released neutrals or, better, of the corresponding deuterons, Γ^0_{D}. In the following analysis we assume that the total particle flux is constant in the limiter temperature range covered in this experiment.

The particle fluxes are not spectroscopically detectable themselves, but rather the photon fluxes of atomic or molecular lines emitted by the respective particles and which are converted from particle fluxes by means of photon efficiency factors, k:

$$\phi^{\mathrm{D}}_{\mathrm{D}} = k_1 \cdot \Gamma_{\mathrm{D}}, \tag{3}$$

$$\phi^{\mathrm{D}_2}_{\mathrm{D}} = k_2 \cdot \Gamma_{\mathrm{D}_2}, \tag{4}$$

$$\phi_{\mathrm{D}_2} = k_3 \cdot \Gamma_{\mathrm{D}_2}. \tag{5}$$

The atomic photon flux $\phi^{\mathrm{D}}_{\mathrm{D}}$ stands for the line emission from excited atoms. This intensity covers different types of energetic atoms, such as the reflected ions, which have only enough residence time to be neutralized on the surface, or thermally released atoms. The atomic photon flux $\phi^{\mathrm{D}_2}_{\mathrm{D}}$ represents the light emission (e.g. Balmer-α) from atoms which come from the molecular dissociation. However, not all molecules are dissociated into two atoms, and, in the steady state case, indeed not all molecules are dissociated. The number of intrinsic atomic photons which arise from those molecules still undissociated is also included in this so-called molecular contribution, $\phi^{\mathrm{D}_2}_{\mathrm{D}}$. The *total* atomic photon flux, ϕ_{D}, is therefore a summation of (3) and (4):

$$\phi_{\mathrm{D}} = \phi^{\mathrm{D}}_{\mathrm{D}} + \phi^{\mathrm{D}_2}_{\mathrm{D}}. \tag{6}$$

In this way the molecular particle flux contributes directly to the atomic line intensity. The individual contributions in (6) to the total intensity can be determined by an external variation in the composition of the particle flux. ϕ_{D_2} stands for the light emission (e.g. Fulcher-α band) from the still undissociated molecules. The molecules can be excited from the electronic ground state and emit light before being ionized or dissociated.

A combination of surface-heating and gas-puff experiments has been proposed in [4] for determining the atomic to molecular flux ratio of hydrogen. Figure 9 shows the corresponding variation of the intensities.

- *Surface heating*: Variation of the limiter temperature leads to a change in the release mechanism of the recycled deuterium (section 3.1). Under constant plasma conditions,

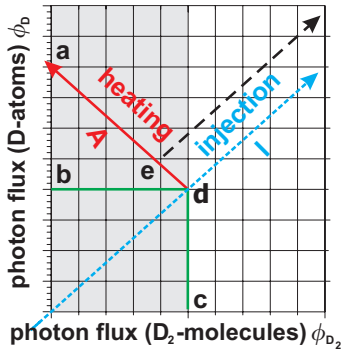

Figure 9. Flux ratio determination: both surface-heating and gas-blow experiments are required if only intensities of atomic and molecular transitions are measured.

the total released deuterium particle flux is constant: $\Gamma_D^0 = \text{const}$. Starting from point **e**, representing an initially unknown ratio of molecules to atoms, one moves along the straight line **A** during the heating process. The intersection with the ordinate **a** represents the photon flux of atomic deuterium when no molecules are left. According to (3) **a** can be rewritten as ϕ_D^0:

$$\phi_D^0 = k_1 \cdot \Gamma_D^0. \tag{7}$$

Using equations (2)–(6), it is a matter of algebra to derive a linear equation relating the atomic and molecular photon fluxes and describing the path **A**:

$$\phi_D = \phi_D^0 + \left[\frac{k_2 - 2k_1}{k_3}\right] \cdot \phi_{D_2}. \tag{8}$$

As we shall see below, it is useful to divide equation (8) by k_1 to get

$$\frac{\phi_D}{k_1} = \frac{\phi_D^0}{k_1} + \beta \cdot \frac{\phi_{D_2}}{k_3} \tag{9}$$

with the definition

$$\beta := \left[\frac{k_2 - 2k_1}{k_1}\right] = \left[\frac{k_2}{k_1} - 2\right]. \tag{10}$$

- *Gas injection*: An additional injection of deuterium gas also allows us to vary the composition. The additional molecular source changes the contributions described by equations (4) and (5). The pure atomic part, equation (3), will not be influenced: $\Gamma_D = \text{const}$. In this scheme, one starts at an unknown point **e** and moves by increasing the amount of injected gas in a direction parallel to the straight line **I**, where **I** is defined by the following equation,

$$\phi_D^{D_2} = \left[\frac{k_2}{k_3}\right] \cdot \phi_{D_2}. \tag{11}$$

The two straight lines represented by equations (8) and (11) intersect at point **d**, whose ordinate and abscissa are given, respectively, by **b**: $(k_2/2k_1)\phi_D^0$ and **c**: $(k_3/2k_1)\phi_D^0$.

Note that from a combination of both experiments under identical plasma conditions the flux ratio can be deduced from simple intensity measurements. Knowledge of the absolute photon fluxes is not necessary for the determination of the atomic to molecular flux ratio [4]. But it is rather challenging to perform both experimental parts—the surface-heating and the gas-puffing

parts—under identical plasma conditions. In particular the gas-puff experiment seems to be critical and can cause larger uncertainties owing to a local disturbance of the plasma. Gas puffing can also lead to a change in the dominant molecular dissociation process [31].

As we shall see below, the use of photon fluxes for the observed molecular and atomic transition allowed a reduction and simplification of the evaluation scheme developed in [4]. The gas-puff experiment can be omitted and the flux ratio can be deduced only from the surface-heating part. Additionally, not only can the flux ratios be determined with the use of photon fluxes, but also the absolute particle fluxes mentioned in equation (2) and the absolute values of the efficiency factor k_2 given in equation (4). This improvement in the analysis scheme was possible thanks to a better treatment of the molecular photon flux of the Fulcher-α band and of the corresponding photon efficiency values [18].

Thus, in the experiments presented here, no gas puffing was performed. The recycled deuterium flux can be obtained from the photon fluxes, ϕ, derived in the surface-heating experimental part. The coefficients k are the photon efficiencies for a certain transition, but their inverse values, S/XB and D/XB, are in common use for atoms and molecules. We can identify k_1^{-1} as S/XB for the directly produced Balmer-α photons, which can be used for a wide parameter range from the ADAS database [33]. By analogy, k_3^{-1} is the D/XB value for the observed Fulcher-band transition. D stands for the decay of the molecules, taking account of the rate coefficients for all possible loss mechanisms (ionization, dissociation). In an ionizing plasma regime, recombination can be neglected. D/XB has been both measured [18, 34] and calculated using a collisional–radiative model [14, 23]. Taking these identities for k_1 and k_3 into account, equation (9) simplifies to

$$\phi_{\mathrm{D}}\left[\frac{S}{XB}\right] = \phi_{\mathrm{D}}^{0}\left[\frac{S}{XB}\right] + \beta \cdot \phi_{\mathrm{D}_2}\left[\frac{D}{XB}\right] \Leftrightarrow \Gamma_{\mathrm{D}}^{*} = \Gamma_{\mathrm{D}}^{0} + \beta \cdot \Gamma_{\mathrm{D}_2}, \tag{12}$$

where $\phi_{\mathrm{D}}^{0}[S/XB]$ has been identified as the total particle flux, Γ_{D}^{0}, and $\phi_{\mathrm{D}_2}[D/XB]$ as the molecular particle flux, Γ_{D_2}. It is also useful for the further discussion to define Γ_{D}^{*} as the measured Balmer-α photon flux, ϕ_{D}, multiplied by the purely atomic quantity S/XB. Γ_{D}^{*} represents an effective flux of the radiating atoms only. By the transformation we change from the photon flux scheme (figure 9) to the particle flux scheme with β as the slope of the new curve **A**, given by the right-hand side of equation (12).

Finally, k_2, which depends on β according to equation (10), has to be determined. k_2 can be written as the product of $\eta = (\beta + 2)$ and k_1. However, k_2 is, according to equation (4), also a conversion factor or photon efficiency. Thus, the factorization of k_2 has a physical meaning: η can be considered as the efficiency for the production of atoms from a molecule and k_1 is the photon efficiency for the emission of a Balmer-α photon from the atoms created in that step. η is determined by the destruction process of the molecule. If dissociation is the initial process, then two atoms are formed; if the destruction starts with ionization and is followed by dissociation of the molecular ion, then only one atom will be produced; and, if two ions are produced directly, then no atom is created and $\eta = 0$ is valid. Here, we assumed that all produced atoms are in the ground state and radiate Balmer photons with efficiency k_1.

This is not necessarily the case for all dissociation processes. Spectroscopically, η stands for the number of Balmer photons from the dissociation of a molecule, where the photon efficiency, k_1, for the created atoms still has to be considered. Thus, a more precise definition for η is the following: η is the efficiency of production of atoms from a molecule which are potentially able to emit Balmer radiation.

Besides this intuitive interpretation, the solution to equation (12) provides values for η and thus for k_2:

$$\eta = (\beta + 2) = \left[\frac{\Gamma_{\mathrm{D}}^{*} - \Gamma_{\mathrm{D}}^{0}}{\Gamma_{\mathrm{D}_2}} + 2 \right] = \frac{k_2}{k_1}. \tag{13}$$

Thus, η is determined experimentally only by the slope, β, in equations (12) and (9). Values for η can be written down directly in the following three simple cases:

- $\eta = 2$: β has to be zero. We obtain $k_2 = 2k_1$.
- $\eta = 1$: Here $\beta = -1$ and $k_2 = k_1$.
- $\eta = 0$: Here $\beta = -2$ and k_2 vanishes.

The experimentally determined η represents an average value over a large number of molecular dissociations with different possible dissociation channels. The values for η lie between the extreme cases.

The change from the intensity to the particle flux scheme (figure 9) now allows the following interpretation of the particle fluxes: the abscissa represents Γ_{D_2} and the ordinate is Γ_{D}^{*}. However, Γ_{D}^{*} is, owing to the molecular contribution $\phi_{\mathrm{D}}^{\mathrm{D}_2}$ to the atomic photon flux ϕ_{D}, in general *neither* the atomic particle flux $\Gamma_{\mathrm{D}} = \phi_{\mathrm{D}}^{\mathrm{D}}[S/XB]$ *nor* the total particle flux Γ_{D}^{0}. We can discuss two extreme cases in the particle flux scheme:

- 0% molecules. The heating of the surface has no influence on the flux. If ϕ_{D_2} is zero then all particles start from the surface as atoms and $\phi_{\mathrm{D}}^{\mathrm{D}}$ is the only contribution to ϕ_{D}. Point **a**: the total particle flux is given by Γ_{D}^{0}, which has been calculated by ϕ_{D}^{0} multiplied by S/XB.
- 100% molecules. Point **e** = **d**: only molecules start from the surface, and $\phi_{\mathrm{D}}^{\mathrm{D}}$ is zero. If the resulting deuterons are counted, then the total particle flux is simply twice the molecular one (**c**). Nevertheless Balmer-α photons can be measured ($\phi_{\mathrm{D}}^{\mathrm{D}_2}$), the number of which only depends on the efficiency value k_2 and thus on η and how many atoms can be created from a molecule. Γ_{D}^{*} is determined by $\phi_{\mathrm{D}}^{\mathrm{D}_2}$ only.

Finally, we can ascertain that, according to equation (12), the total flux, Γ_{D}^{0}, can be determined by means of the particle flux Γ_{D_2}, Γ_{D}^{*} and the slope β or, better, the efficiency η.

4.2. Analysis of the experimental results

For series 2, Γ_{D}^{*}, the Balmer-α photon flux (section 3.1) multiplied by the S/XB value for the pure atomic case ($S/XB = 15.17$), is plotted in figure 10 versus Γ_{D_2}, the total Fulcher-band photon flux multiplied by the corresponding D/XB value ($D/XB = 2000$). The conversion into the pure atomic flux, Γ_{D}, is only valid on the ordinate, where Γ_{D_2} vanishes. Up to the threshold value of $T_{\mathrm{TL}} = 1100$ K, practically no variation of the composition can be observed (point **e**). In analogy to line **A**, an experimental curve can be established which is defined by the linear increase in the atomic contribution and the decrease in the molecular contribution caused by further heating of the limiter. The slope, β, of this experimental curve is almost -1 and thus the efficiency, η, is nearly 1. The intersection of the extrapolation of this line with the ordinate defines the photon flux corresponding to point **a** in figure 9, where Γ^{tot} is determined by the pure atomic flux. We can deduce the pure atomic contribution, Γ_{D}, according to equation (2) by subtracting Γ_{D_2} from the previously determined Γ^{tot}. The variation of Γ_{D} within experimental series 2 is depicted in figure 10 as a bar chart on top.

Figure 11(*a*) shows the variation of the atomic and molecular contributions to Γ^{tot} for discharge series 2 as a function of T_{TL}. Up to the threshold temperature of 1100 K, about 90% of the deuterium starts as molecules from the surface. The remaining 10% can be attributed

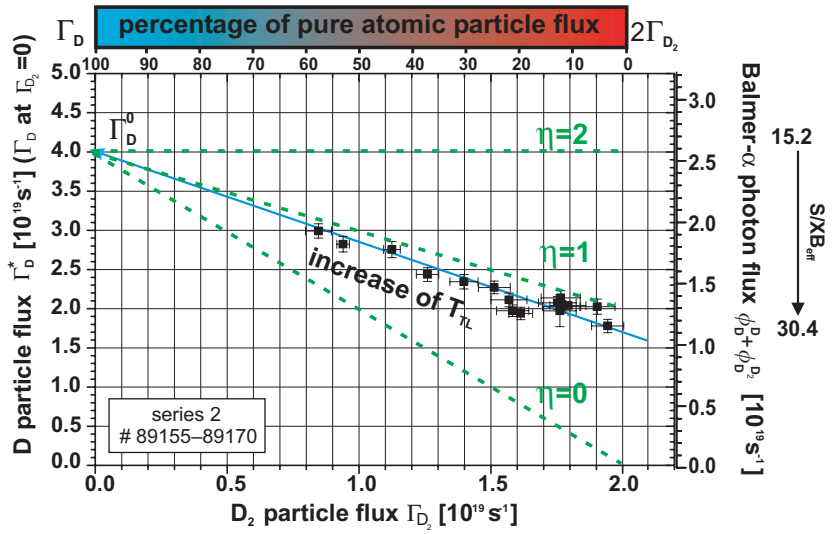

Figure 10. #89155–70. Determination of Γ^{tot} from the surface heating experiment in TEXTOR. The abscissa represents the previously defined Γ_D^*. The slopes for the cases $\eta = 0, 1, 2$ are marked as a reference.

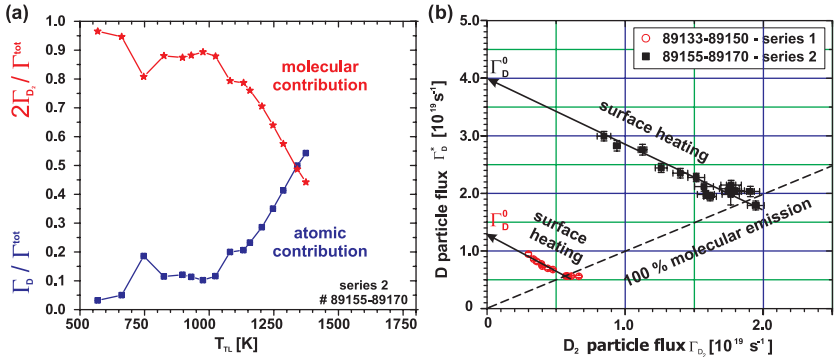

Figure 11. (*a*) #89155–70. Variation of the molecular and atomic contributions to the deuterium particle release during the heating phase. (*b*) Comparison of the behaviour for the two discharge series (see table 1).

to reflected atoms. The increase in the limiter temperature forces a strong change in the composition, so that by $T_{TL} = 1350$ K an equal contribution of molecules and atoms to the particle release is reached. Extrapolation to higher limiter temperatures predicts a pure atomic release above $T_{TL} \simeq 1700$ K.

Finally, figure 11(*b*) shows a comparison between the two discharge series, where $S/XB = 14.13$ and $D/XB = 2200$ have been used as conversion factors for series 1. The behaviour of the two series is similar, although the molecular correction seems to be a little higher for the higher electron temperature (series 1), and the efficiency factor is lower. Additionally, the straight line **I** is determined by the starting values of both series for temperatures below the threshold.

Apart from the flux determination which was the main aim of these experiments, the question about the dominant electron impact-induced dissociation process for $T_{TL} < 1700$ K

remains. The particle flux determination indicates that about half of the expected Balmer-α radiation and also half of the Balmer-γ radiation (section 3.3) are missed. This can be interpreted as the absence of about half of the atoms which would favour the dissociation process of type (ii) via the break-up of the molecular ion where one atom and one ion are built. Note that for this process $\eta = 1$ represents a strict upper limit. But the dissociation into two atoms (type (iii)), where one atom does not emit Balmer radiation, might also lead to a lack of Balmer photons. This dissociation process has no strict upper limit of $\eta = 1$ but would allow values above 1. And indeed, in [31] it is mentioned that both atoms, the excited one and the one in the ground state, contribute to the Balmer radiation for similar plasma conditions. The edge plasma is most probably characterized by a mixture of the concurrent processes.

However, reaction (ii) is the dominant one in the high temperature edge plasma of TEXTOR ($T_e > 30\,eV$) if one takes into account the rate coefficients[4] for the different dissociation process [35, 36]. A definite answer about the processes cannot be given within this work, but probably only in a simulation with a neutral particle code which includes a collisional–radiative model for deuterium [37].

4.3. Effective S/XB values for Balmer-α

In general Γ^{tot} cannot be determined from the Fulcher-band and the Balmer-α photon flux without additional information about η and the number of atoms, which are released as such on the surface. Nevertheless, in the case of the not actively heated limiter in TEXTOR, we are able—with the measurements presented in the previous section—to determine Γ^{tot} from the line emission of Balmer-α. We can introduce an effective $(S/XB)_{eff}$ value which takes into account the molecular contribution in the conversion value empirically and thus 'corrects' the measured Balmer-α photon flux, ϕ_D:

$$\Gamma^{tot} = \left(\frac{S}{XB}\right)_{eff} \cdot \phi_D. \tag{14}$$

$(S/XB)_{eff}$ is not constant but depends on the molecular flux, or more precisely, implicitly on the ratio of molecular to atomic flux. $(S/XB)_{eff}$ may be written as

$$\left(\frac{S}{XB}\right)_{eff} = \frac{S}{XB} + k_2^{-1}\left[\frac{2\Gamma_{D_2}}{\Gamma^{tot}}\right] = \frac{S}{XB}\left(1 + \eta^{-1}\left[\frac{2\Gamma_{D_2}}{2\Gamma_{D_2} + \Gamma_D}\right]\right), \tag{15}$$

where η is nearly 1 under the conditions of our experiment. The variation in this conversion value for series 2 is given on the right scale of figure 10. The appropriate value for $(S/XB)_{eff}$ is about 30 for the not actively heated limiter, which is nearly twice the original S/XB value.

Note that the measurement of the Balmer-α photon flux alone and the use of the original conversion factor S/XB may not provide Γ^{tot} if a molecular particle flux is present. Confusion of Γ_D^* for Γ^{tot} would, according to equation (12), lead to an underestimate of the total recycling flux.

5. Summary and conclusion

The externally pre-heated graphite limiter, which allows control of the surface temperature independently of the plasma conditions, proves to be a powerful tool for development of spectroscopic means of determining the recycling particle fluxes and the deuterium release mechanisms. The variable surface temperature in particular influences the fraction of particles

[4] A full set of the different possible dissociation processes with its rate coefficients in dependence on the plasma parameters n_e and T_e can be found in the atomic and molecular database of the EIRENE code [37].

being released as molecules or atoms. This fact is used to develop a spectroscopic method—based on inverse photon efficiencies—in order to disentangle the various particle fluxes related to molecules or atoms. For a full treatment of the deuterium recycling, the Fulcher-band photon flux, the Balmer-α photon flux and the efficiency factor (η), which gives the average number of potentially radiating atoms originating from molecular dissociation, were measured.

We also determined the main properties of the species released from cold and hot graphite surfaces, such as the energy composition and penetration depth of the atoms and the rotational and relative vibrational populations of the molecules. The resulting data show significant variations with the surface temperature, as summarized in the following.

Cold surface. From $T_{\mathrm{TL}} = 570\,\mathrm{K}$ to $T_{\mathrm{TL}} = 1100\,\mathrm{K}$ the main fraction of deuterium particles (90%) starts as molecules from the graphite surface. Analysis of the rotational population indicates that the release of the molecules is mainly thermal. Only about 10% of the directly released particles are atoms. These atoms have relatively high energies of the order of the background ions. However, according to the Zeeman analysis, about 90% of the measured Balmer-α photons correspond to two other types of atoms with energies around 0.3 and 3.3 eV. Both energies are related to the dissociation of molecules. η is determined for these surface conditions to be about 1. This reflects the fact that only *one* potentially radiating atom will be effectively produced from a molecule. Dissociation via the molecular ion D_2^+ is one of the probable mechanisms among several possibilities.

Hot surface. At the highest graphite temperatures, $T_{\mathrm{TL}} > 1700\,\mathrm{K}$, the particle release produces atoms only. Molecules are no longer released from the surface. Since recombination of atoms in the TEXTOR plasma parameter range can be neglected, in this case Balmer-α is solely due to atoms released directly into the plasma. According to the line profile analysis of Balmer-α, these atoms are mainly thermal and reflect the graphite surface temperature. These thermal atoms have a short penetration depth and their maximum of emission is located directly in front of the limiter, as the radial distribution of Balmer-γ shows.

Intermediate case. The release behaviour changes continuously from molecular to atomic recycling fluxes between $T_{\mathrm{TL}} = 1100\,\mathrm{K}$ and $T_{\mathrm{TL}} = 1700\,\mathrm{K}$.

In the case of the not actively heated limiter, and thus for standard PFCs made of graphite, this leads to consequences in the total particle flux determination if only the Balmer-α photon flux with the standard S/XB value is considered. Without consideration of the surface-released molecules and $\eta \simeq 1$, it would give—with respect to the resulting deuterons—a flux which is too small by a factor of nearly 2. On this basis, effective inverse photon efficiencies have been introduced—thus taking into account different ratios of molecules and atoms—to obtain the recycling deuterium flux for mixed cases from Balmer-α. The use of these $(S/XB)_{\mathrm{eff}}$ values leads to a significant improvement of the standard spectroscopic method, which is based on the assumption that only atoms are present and that the role of deuterium molecules in the recycling process is negligible.

References

[1] Federici G *et al* 2001 *Nucl. Fusion* **41** 12
[2] Philipps V *et al* 2000 *Plasma Phys. Control. Fusion* **42** B293

[3] Pospieszczyk A *et al* 1997 *24th EPS Conf. on Controlled Fusion and Plasma Physics (Berchtesgarden)* vol 21A (ECA) p 1733
[4] Pospieszczyk A *et al* 1999 *J. Nucl. Mater.* **266–269** 138
[5] McNeill D H 1989 *J. Nucl. Mater.* **162–164** 476
[6] Stangeby P C and McCracken G M *Nucl. Fusion* **30** 1225
[7] Samm U *et al* 1999 *Plasma Phys. Control. Fusion* **41** B57
[8] Mertens Ph *et al* 2001 *Plasma Phys. Control. Fusion* **43** A349
[9] Reiter D 2005 Modelling of fusion edge plasmas: atomic and molecular data issues *Nuclear Fusion Research: Understanding Plasma–Surface Interaction* vol 78, ed R E H Clark and D Reiter (Berlin: Springer)
[10] Pospieszczyk A 1993 Diagnostics of edge plasmas by optical methods *Atomic and Plasma-Material Interaction Processes in Controlled Thermonuclear Fusion* ed R K Janev and H W Drawin (Amsterdam: Elsevier)
[11] Fantz U and Heger B 1998 *Plasma Phys. Control. Fusion* **40** 2023
[12] Brezinsek S *et al* 2001 *28th EPS Conf. on Controlled Fusion and Plasma Physics (Funchal)* vol 25A (ECA) p 2077
[13] Greenland P T 2002 *Contrib. Plasma Phys.* **42** 608
[14] Wünderlich D 2001 *IPP-Report 10/18* Max-Planck-Institut für Plasmaphysik, Garching
[15] Samm U *et al* 1989 *J. Nucl. Mater.* **162–164** 24
[16] Brezinsek S 2002 *Jül-Bericht 3962* (Jülich: Forschungszentrum Jülich) ISSN 0944-2952
[17] Mertens Ph *et al* 1997 *J. Nucl. Mater.* **241–243** 842
[18] Brezinsek S *et al* 2003 *J. Nucl. Mater.* **313–316** 967
[19] Schweer B *et al* 1999 *J. Nucl. Mater.* **266–269** 637
[20] Kreter A *et al* 2000 *27th EPS Conf. on Controlled Fusion and Plasma Physics (Budapest)* vol 24B (ECA) p 1232
[21] Franzen P and Vietzke E 1994 *J. Vac. Sci. Technol.* A **12** 820
[22] Fantz U 2002 *IPP-Report 10/21* Max-Planck-Institut für Plasmaphysik, Garching
[23] Greenland P T 2001 *Proc. R. Soc. Lond.* **457** 1821
[24] Brezinsek S *et al* 2002 *Contrib. Plasma Phys.* **42** 668
[25] Lavrov B P *et al* 1980 *J. Appl. Spectrosc.* **32** 316
[26] Mertens Ph and Pospieszczyk A 1999 *J. Nucl. Mater.* **266–269** 884
[27] Brezinsek S *et al* 2003 *Phys. Scr.* **T103** 51
[28] Huber A *et al* 2001 *J. Nucl. Mater.* **290–293** 276
[29] Hey J D *et al* 1996 *Contrib. Plasma Phys.* **36** 583
[30] Hey J D *et al* 1999 *J. Phys. B: At. Mol. Opt. Phys.* **32** 3555
[31] Hey J D *et al* 2004 *J. Phys. B: At. Mol. Opt. Phys.* **37** 2543
[32] Reiter D *et al* 1992 *J. Nucl. Mater.* **196–198** 1059
[33] http://adas.phys.strath.ac.uk
[34] Fantz U *et al* 2003 *J. Nucl. Mater.* **313–316** 743
[35] Janev R *et al* 2003 *Jül-Bericht 4105* (Jülich: Forschungszentrum Jülich) ISSN 0944-2952
[36] Janev R 1987 *Elementary Processes in Hydrogen-Helium Plasmas* (Berlin: Springer)
[37] http://www.eirene.de